Characterizing the Quenching Process for Phosphorescent Dyes in Poly[((*n*-butylamino)thionyl)phosphazene] Films

Xin Lu, Bao-Hang Han, and Mitchell A. Winnik*

Department of Chemistry, University of Toronto, 80 St. George Street, Toronto, ON M5S 3H6, Canada

Received: July 31, 2003; In Final Form: September 18, 2003

We compare the results of oxygen quenching experiments for four phosphorescent dyes [platinum octaethylporphyrin (PtOEP), platinum octaethylporphyrin ketone (PtOEPK), platinum tetrakis(pentafluorophenyl)porphyrin (PtTFPP), and $Ru(dpp)_3Cl_2$ (dpp = 4,7-diphenyl-1,10-phenanthroline)] in a low-glass-transition-temperature polymer matrix [poly[((*n*-butylamino)thionyl)phosphazene] (C_4PATP).] The Pt dyes have exponential unquenched decays, but nonexponential decays in the presence of O_2. These data fit well to a two-site model in which the dyes in the short lifetime environment are more readily quenched by oxygen. $Ru(dpp)_3Cl_2$ in C_4PATP has a nonexponential decay under all conditions and is much better described by a Gaussian distribution of decay rates with a common mean quenching rate. Time-scan experiments with PtOEP, PtTFPP, and $Ru(dpp)_3Cl_2$ gave very similar values for the diffusion coefficient for oxygen in the polymer (D_{O_2} = (3.7−4.0) × 10^{-6} cm^2 s^{-1}). For each of these three dyes, lifetimes and intensities gave identical Stern−Volmer plots. From the slopes of these plots one can calculate the permeability P_{O_2} and solubility S_{O_2} = P_{O_2}/D_{O_2} of oxygen in the matrix. In this calculation, one must assume a value (commonly taken to be 1.0 nm) for αR_{eff}, the probability of quenching per encounter times the effective quenching radius of the dye. We find differences in calculated P_{O_2} values that can only be explained in terms different sensitivities of the dyes to quenching by oxygen.

Introduction

Phosphorescent dyes in polymer matrixes are used as oxygen sensors.[1,2] One normally studies the kinetics of quenching by oxygen as a means of obtaining the parameters that characterize oxygen diffusivity (D_{O_2}), solubility (S_{O_2}), and permeability (P_{O_2} = $D_{O_2}S_{O_2}$) in the matrix.[3] In this way one builds the knowledge base for sensor optimization.

In this paper, we approach the issue of oxygen quenching from a more fundamental perspective. We are interested in the influence of the polymer matrix on the quenching process, comparing four different dyes. Dyes in solution normally exhibit exponential decays, in both the absence and presence of quenchers.[4] The same dyes in glassy polymer matrixes, even in the absence of quencher, are often characterized by nonexponential decays. In solution, density fluctuations relax faster than the excited-state lifetime. Thus each excited-state experiences the same time-averaged environment. In glasses, these fluctuations are frozen. Different dye molecules find themselves in somewhat different environments, and their excited states decay at different rates.

Polymers well above their glass transition temperature (T_g) are viscoelastic fluids in which quencher diffusion depends on the rate of free volume relaxation. This rate is related to local chain dynamics rather than the bulk viscosity of the system. In these viscoelastic fluids, nonionic dyes commonly exhibit exponential luminescence decay profiles. Much less is known about how the dye and matrix interact to affect processes such as oxygen quenching. Here we examine oxygen quenching for four different dyes in a common low T_g polymer matrix. The matrix consists of a relatively high molar mass (M_w = 1.6 × 10^5; PDI = 2.3) sample of poly[((*n*-butylamino)thionyl)-phosphazene] (C_4PATP). This polymer was first synthesized by Manners and co-workers.[5] The backbone of this polymer is made up of sulfur, nitrogen, and phosphorus atoms. The local dipoles make this polymer an excellent medium for dissolving dyes, and the large S−N−P and P−N−P bond angles contribute to the chain flexibility, and thus, to the observed low values of the glass transition temperature (T_g).[6] Previous work in our laboratory indicates that this polymer is an excellent matrix for phosphorescent oxygen sensors.[7,8] The structures of the polymer and of the four dyes, platinum octaethylporphyrin (PtOEP), platinum octaethylporphyrin ketone (PtOEPK), platinum tetrakis(pentafluorophenyl)porphyrin (PtTFPP) and ruthenium tris-(4,7-diphenyl-1,10-phenanthroline) dichloride ($Ru(dpp)_3Cl_2$), are shown in Chart 1.

We find, as expected, that the platinum porphyrin dyes have exponential decays in C_4PATP, whereas the decay of $Ru(dpp)_3Cl_2$ is nonexponential. What is surprising is that all four dyes show nonexponential decays in the presence of oxygen, and different models are needed to describe the behavior of the charged and neutral dyes. In addition, the dyes vary in the efficiency with which a single diffusive encounter with oxygen results in a quenching event.

Experimental Section

Materials. Poly[((*n*-butylamino)thionyl)phosphazene] (C_4-PATP, M_w = 1.6 × 10^5, PDI = 2.3) was obtained from the Manners research group. Platinum octaethylporphyrin (PtOEP), platinum octaethylporphyrin ketone (PtOEPK), and platinum tetrakis(pentafluorophenyl)porphyrin (PtTFPP) were purchased from Porphyrin Products Inc. (Logan, UT) and used without further purification. $[Ru(dpp)_3]Cl_2$ (dpp = 4,7-diphenyl-1,10-phenanthroline) was synthesized in Prof. Manners' group according to the procedure described by Lin et al.[9] The chemical structures of the polymer and dyes are shown in Chart 1.

10.1021/jp036245q CCC: $25.00
Published on Web 11/11/2003

CHART 1

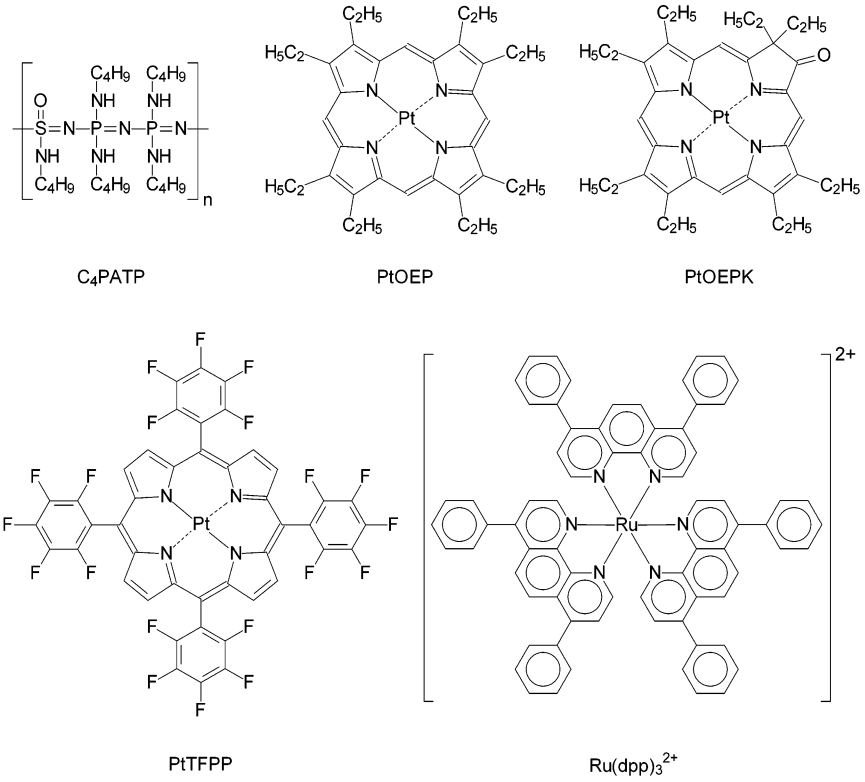

Preparation of Dye-Containing Polymer Films. A polymer solution containing 0.5 g of C_4PATP and 0.05 mg of dye in 10 mL of 1,1,1-trichloroethane was cast onto a cut glass microscopic slide (2.0 cm × 1.3 cm × 0.1 cm). The slide was placed in a covered container with a small opening in order to slow the solvent evaporation rate. The container was then stored in the dark at room temperature for 1 day. The dense film on its substrate was then transferred to a vacuum oven. It was heated at 60 °C at ambient pressure for 24 h, followed by annealing at 60 °C under vacuum (<1 Torr) for 48 h. With this procedure, we can remove solvent from sample films without creating voids or air bubbles. The coated glass slide was then allowed to cool to room temperature (22 °C). The film thickness was determined with a Mitutoyo thickness gauge.

Luminescence Measurements. For steady-state phosphorescence measurements, a film-coated glass substrate was placed in a closed sample chamber. The whole chamber with its pressure/temperature-control accessories was fitted into the optical path of a SPEX Fluorolog II spectrometer equipped with a DMA 3000 data system. The slits for the excitation/emission light beams were set between 0.5 and 1.5 mm depending on the thickness of the film used. The intensity of the emitted light was monitored at a right angle relative to the excitation light, and the intensity signals were recorded in the S/R mode (sample source signal divided by reference signal) in 0.5 nm steps. For the linearity of response, the sample source signal was always kept to less than 2×10^5 count s^{-1}. Prior to each intensity measurement, the sample was monitored in the sample chamber for sufficient time (typically 5 min for a film with a thickness of 100 μm) for the emission signal to become stable. The air pressure inside the chamber was controlled over a range from 0 to 760 Torr (1 atm = 760 Torr) through a combination of a vacuum pump and a compressed gas line. Gas pressure was measured by a Matheson standard absolute pressure gauge (0−760 Torr with an accuracy of ±2 Torr) and a MKS Baratron 626A absolute pressure transducer (0−120 Torr with an accuracy of ±0.25% of the reading).

Time-scan experiments were carried out to monitor the change of emission intensity as a function of time after a dye-containing polymer film was exposed to a step-change of air pressure. Here the sample chamber was replaced by a small fluorescence cell (3.0 cm × 1.0 cm × 1.0 cm) covered by a rubber septum cap. A film supported by a glass substrate was mounted in the cell. Two syringe needles pierced the cap to allow gases (nitrogen, compressed air) to flow in to and out of the cell. Initially, the cell was flushed with nitrogen until virtually all of the oxygen was removed from the film as noted by the constant luminescence emission intensity (at its most intense value). At this point, the oxygen concentration was assumed to be zero both inside and outside of the film, and the emission intensity $I = I°$ ($p_{O_2} = 0$ atm). At time zero, the film was at once exposed to 1 atm air ($p_{O_2} = 0.21$ atm). Inside the film, the oxygen concentration increased to its final uniform equilibrium value, and concurrently the measured emission intensity dropped to its final value I_{eq}. This oxygen "diffusion-in" experiment is an oxygen-sorption experiment. The same sample film was then ready for an oxygen-desorption experiment. The external pressure of oxygen was at once brought to zero by flushing the cell with nitrogen. There was a net diffusion of quenchers (oxygen) out of the sample, until the oxygen concentration was nearly zero everywhere in the film. The measured intensity concurrently increased from I_{eq} to $I°$. Since the gas flow rates in these experiments were greater than 100 cm^3 s^{-1}, the fluorescence cell (volume = 3 cm^3) can be flushed out by the second gas in less than 0.03 s. Compared to the much longer time for gas diffusion through polymer films, the time for gas exchange has little effect on the time-scan experiments.

Luminescence decay profiles of excited state dyes were measured by using the second harmonic of a Nd:YAG laser (Spectra Physics DCR 2) at 532 nm with a pulse width of 10

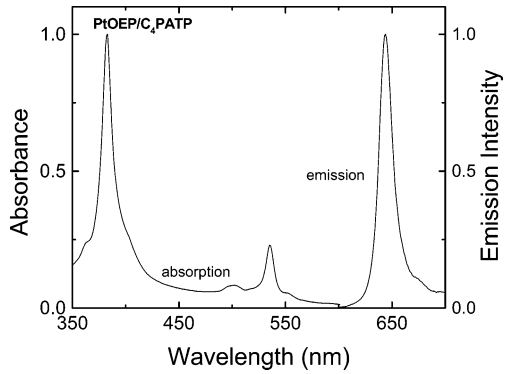

Figure 1. Normalized absorption and emission spectra of PtOEP (100 ppm) in a C_4PATP film in a nitrogen atmosphere.

ns as the excitation source. The beam intensity was severely attenuated to prevent sample damage and dye photobleaching. Following sample excitation, the phosphorescence of the dye in the polymer films was detected by a Hammamatsu 956 photomultiplier tube connected to a Tektronix model 1912 transient digitizer. The decay trace was then transferred to a computer for analysis.

Data Analysis. A detailed description of the theory of the data analysis for both time-scan and time-resolved experiments has been presented in previous publications.[10] Here we briefly summarize the fundamental ideas and the equations required for data analysis in this paper.

The kinetics of luminescence quenching involving mobile quenchers is described by the Stern−Volmer equation.[4] For experiments involving oxygen as the quencher in polymer films above T_g, we can write

$$\frac{I^\circ}{I} = \frac{\tau^\circ}{\tau} = 1 + 4\pi\alpha R_{\text{eff}} N_A \tau^\circ D_{O_2}[O_2]_{\text{eq}} = 1 + 4\pi\alpha R_{\text{eff}} N_A \tau^\circ D_{O_2} S_{O_2} p_{O_2} \quad (1)$$

In this expression, I° is the emission intensity and τ° is the dye lifetime in the absence of quencher. N_A is Avogadro's number, and I is the emission intensity for a sample containing a bulk-average molar quencher concentration $[O_2]$. The subscript "eq" in eq 1 is used to emphasize the requirement that when the quencher is a gas (i.e., oxygen); it must be in equilibrium with the condensed phase in which the quenching reaction occurs. Hence, $[O_2]_{\text{eq}}$ can also be replaced by the product of oxygen solubility (S_{O_2}) and its partial pressure (p_{O_2}). The term α describes the probability that an encounter of a dye and a quencher will result in deactivation of the dye excited state. R_{eff} is an effective interaction distance at which diffusion-controlled quenching takes place. In our time-scan experiments, a parameter of B is defined in terms of the limiting luminescence intensities in the absence of oxygen and in the presence of 1 atm air and is used to calculate the oxygen permeability ($P_{O_2} = D_{O_2}S_{O_2}$) in the polymer.

$$B = \frac{I^\circ}{I_{1\text{atm air}}} - 1 = 4\pi\alpha R_{\text{eff}} N_A \tau^\circ (D_{O_2} S_{O_2})(0.21 \text{ atm}) \quad (2)$$

When oxygen diffuses through a dye-containing polymer film, one can "divide" the film into a series of parallel layers that are perpendicular to the diffusion direction. If these layers are sufficiently thin, we can assume that the *local concentration* of oxygen ($[O_2](x,t)$), in the layer located between x and $x + \delta x$ at time t, is essentially uniform. For a film (with a thickness of L) coated on a gas-impermeable substrate, the relative oxygen

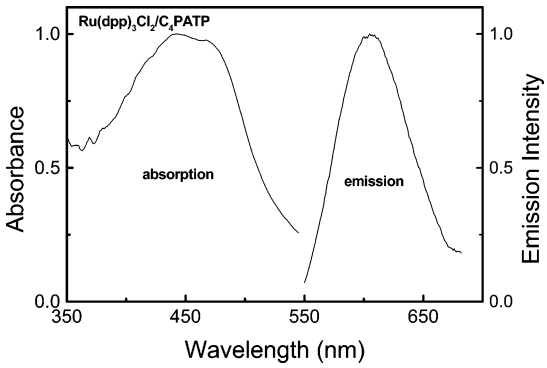

Figure 2. Normalized excitation and emission spectra of $Ru(dpp)_3Cl_2$ (100 ppm) in a C_4PATP film in a nitrogen atmosphere.

concentration $\rho(x,t)$ is defined as the ratio of $[O_2](x,t)$ to $[O_2]_{\text{eq}}$ when the film is in equilibrium with 1 atm air.

Oxygen sorption:

$$\rho(x,t) = 1 - \frac{4}{\pi}\sum_{n=\text{odd}}^{\infty}\frac{1}{n}\exp\{-n^2\pi^2 D_{O_2} t/4L^2\}\sin(n\pi x/2L) \quad (3a)$$

Oxygen desorption:

$$\rho(x,t) = \frac{4}{\pi}\sum_{n=\text{odd}}^{\infty}\frac{1}{n}\exp\{-n^2\pi^2 D_{O_2} t/4L^2\}\sin(n\pi x/2L) \quad (3b)$$

Simultaneously, the quenched phosphorescence intensity of excited dye molecules in each thin layer, $\delta I(x,t)$, can be described as a Stern−Volmer-type equation

$$\frac{\delta I^\circ}{\delta I(x,t)} = 1 + B\frac{[O_2](x,t)}{[O_2]_{\text{eq}}} \qquad \delta I^\circ = I^\circ\, dx/L \quad (4a)$$

$$I(t) = \frac{I^\circ}{L}\int_0^L \frac{dx}{1 + A[O_2](x,t)} \quad (4b)$$

If the values of D_{O_2} and L both are known, one can replace the $[O_2](x,t)$ term in eq 4a by eq 3 and then integrate it to calculate the time profile of the emission intensity from the tested film. The result of this calculation is a *simulated* intensity vs time profile. One can also simulate curves using measured values of B and L and arbitrarily chosen values of D_{O_2}. The diffusion coefficient is treated as an adjustable parameter in comparing simulated $I(t)$ profiles with those measured experimentally. The best fit can be obtained by a minimization of the goodness-of-fit parameters χ^2 in the least-squares analysis.

Results

The absorption and emission spectra of PtOEP (100 ppm) dissolved in a C_4PATP film are plotted in Figure 1. In the absorption spectrum there are two bands, due to $^1S_0 \rightarrow {}^1S_1$ (π, π^*) transition at 537 and 504 nm, and a near-ultraviolet absorption band $^1S_0 \rightarrow {}^1S_2$ (π, π^*) at 383 nm. Here $^1S_0$ refers to the closed-shell ground state, and $^1S_1$, $^1S_2$ are the first and second lowest excited singlet states. The UV−vis absorption spectrum of PtTFPP in C_4PATP resembles that of PtOEP in C_4PATP, but the band positions of PtTFPP are red-shifted by a few nanometers (392, 507, and 541 nm). In C_4PATP, the maximum emission of PtTFPP is located at 649 nm, which is 4 nm longer than that of PtOEP. We present the UV−vis absorption and emission spectra of $Ru(dpp)_3Cl_2$ in a C_4PATP film in Figure 2. There is a broad absorption peak located

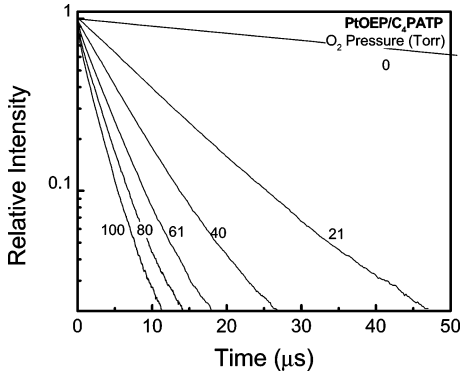

Figure 3. Phosphorescence decay profiles of PtOEP (100 ppm) in a C_4PATP film at various oxygen pressures.

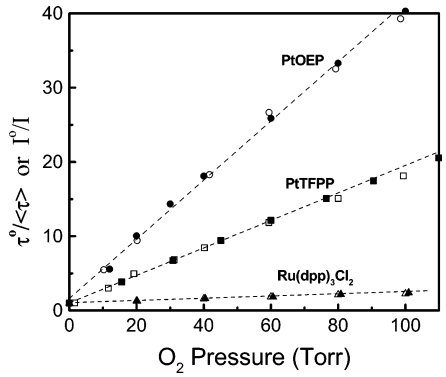

Figure 4. Lifetime (open symbols) and intensity (filled symbols) Stern−Volmer plots for oxygen quenching of three different dyes (PtOEP, PtTFPP, and $Ru(dpp)_3Cl_2$) in C_4PATP. The slopes of plots are proportional to the product of oxygen permeability and the unquenched dye lifetime.

between 400 and 500 nm. The emission band of $Ru(dpp)_3Cl_2$ in C_4PATP has its maximum at 605 nm.

Time-Resolved Experiments. Phosphorescence decays following pulsed excitation of PtOEP dissolved in a C_4PATP film ([PtOEP] = 100 ppm) are shown in Figure 3. In the absence of oxygen, the decay profile is exponential. From the plot we calculated the "unquenched" lifetime ($\tau°$) of PtOEP to be 102 μs. The decay profiles in the presence of oxygen are no longer exponential. To calculate the average lifetime of PtOEP at various oxygen pressures, the decays were fitted to a sum of two exponential terms:

$$I(t) = \sum_i A_i \exp(-t/\tau_i) \qquad i = 2 \tag{5}$$

Values of the average lifetime ($\langle\tau\rangle$, $\sum_i A_i = 1$) were calculated as

$$\langle\tau\rangle = \sum_i A_i \tau_i \qquad i = 2 \tag{6}$$

The pressure dependence of $\langle\tau\rangle$ is shown in Figure 4. The values of $\tau°/\langle\tau\rangle$ increase linearly with oxygen pressure, with a slope of 0.39 $Torr^{-1}$. The intensity ratios ($I°/I$) of PtOEP in C_4PATP were measured in steady-state experiments. These values are also plotted in Figure 4. This intensity Stern−Volmer plot is in good agreement with the lifetime Stern−Volmer plot.

Time-resolved phosphorescence decay profiles for oxygen quenching of PtTFPP in C_4PATP are shown in Figure 5. In the absence of oxygen, the exponential decay gives a value of $\tau° = 66 \pm 2$ μs, similar to that for PtOEPK (64 μs). Both of these values are shorter than that of PtOEP in C_4PATP (102 ± 3 μs).

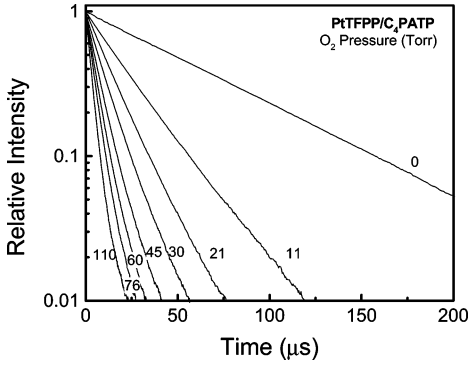

Figure 5. Phosphorescence decay profiles of PtTFPP (100 ppm) in a C_4PATP film at various oxygen pressures.

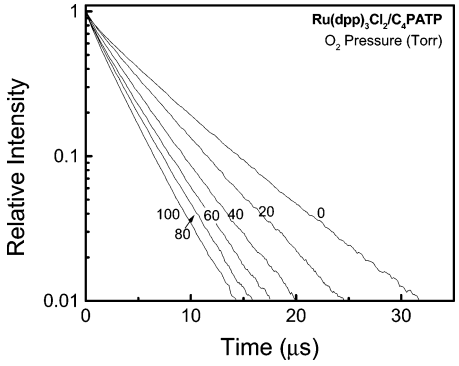

Figure 6. Phosphorescence decay profiles of $Ru(dpp)_3Cl_2$ (100 ppm) in a C_4PATP film at various oxygen pressures.

As the oxygen pressure is increased, the decay profiles of PtTFPP become nonexponential. The average lifetimes of PtTFPP were calculated and compared with those of PtOEP in Figure 4. Plots of $\tau°/\langle\tau\rangle$ and $I°/I$ vs p_{O_2} are linear and coincident for PtTFPP, with a slope of 0.17 $Torr^{-1}$, about half value for PtOEP.

The ionic dye $Ru(dpp)_3Cl_2$ has a nonexponential luminescence decay in the absence of oxygen (Figure 6). When oxygen is present, the decay rate is increased, but the magnitude of quenching by oxygen (Figure 6) is not as great as that for PtOEP (Figure 3) and PtTFPP (Figure 5). The decays in Figure 6 were fitted to a sum of two exponential terms to calculate their average lifetimes in terms of eqs 5 and 6. The unquenched average lifetime is 6.2 μs, one-fifteenth that of PtOEP. Both lifetime and intensity Stern−Volmer plots (Figure 4) for oxygen quenching of $Ru(dpp)_3Cl_2$ in C_4PATP agree well in the p_{O_2} range of 0−100 Torr. The slope of this plot (0.013 $Torr^{-1}$) is substantially smaller than that of PtOEP (0.39 $Torr^{-1}$), PtOEPK (0.22 $Torr^{-1}$), or PtTFPP (0.17 $Torr^{-1}$).

Time-Scan Experiments. We have previously reported time-scan experiments for PtOEP in C_4PATP.[7] The new experiments reported here are provided for completeness in comparing the behavior of PtOEP with that of the other two dyes. Examples of intensity profiles obtained from time-scan experiments are shown for PtOEP/C_4PATP in Figure 7, for PtTFPP/C_4PATP in Figure 8, and for $Ru(dpp)_3Cl_2$/C_4PATP in Figure 9. In Figure 7a, we see that the relative intensity of PtOEP emission starts to increase slowly at time zero, when nitrogen at 1 atm flushes an air-filled fluorescence cell containing the PtOEP/C_4PATP film. The increased intensity becomes stable after ca. 180 s.

A simulated profile of intensity versus time is also plotted in Figure 7a (dashed curve), which is obtained through eqs 1−4 with D_{O_2} as an adjustable parameter. When 1 atm air is rapidly flushed into the system, the intensity starts to drop very fast

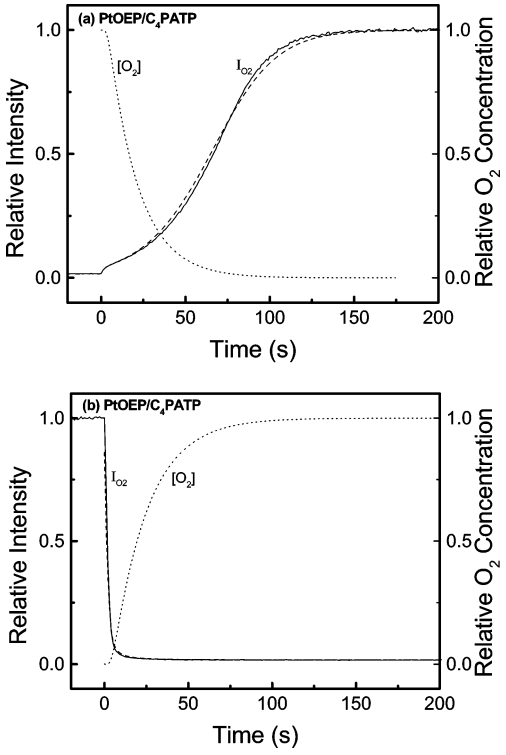

Figure 7. Intensity profiles of oxygen desorption (a) and sorption (b) obtained from the time-scan experiments on PtOEP (100 ppm) in a C_4PATP film (0.125 mm thick) The solid curves refer to experimental data, whereas the overlapping dashed line were simulated using assumed values of D_{O_2} (sorption, $D_{O_2} = 3.58 \times 10^{-6}$ cm^2 s^{-1}; desorption, $D_{O_2} = 3.06 \times 10^{-6}$ cm^2 s^{-1}). The plots of oxygen concentration were obtained with these values of D_{O_2} by integrating eq 3b over the film thickness.

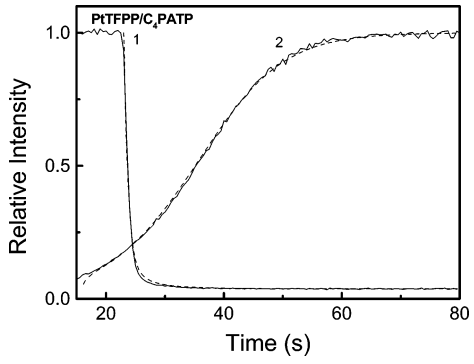

Figure 8. Time-scan plots of the luminescent intensity of PtTFPP in a C_4PATP film on glass as a function of time. The emission was monitored at 649 nm during steady-state excitation at 539 nm. The experimental data (continuous curve) are compared with data simulated (dashed curve) using $D_{O_2} = 4.1 \times 10^{-6}$ cm^2 s^{-1} for oxygen sorption (curve 1) and $D_{O_2} = 3.9 \times 10^{-6}$ cm^2 s^{-1} for oxygen desorption (curve 2).

(Figure 7b). The intensity decreases in the first 25 s by around 90%, compared to the more than 100 s needed for the intensity growth in the corresponding oxygen-desorption experiment shown in Figure 7a. This big difference in response time is a consequence of the coupling of Stern−Volmer quenching and Fick's law of diffusion. One obtains nearly identical values of oxygen diffusion coefficients in oxygen-desorption and -sorption experiments. From 18 experiments with films of varying thickness, we obtain an average value of $D_{O_2} = (3.7 \pm 1.0) \times 10^{-6}$ cm^2 s^{-1}. The reproducibility of results is much better when the measurements are performed on the same film sample

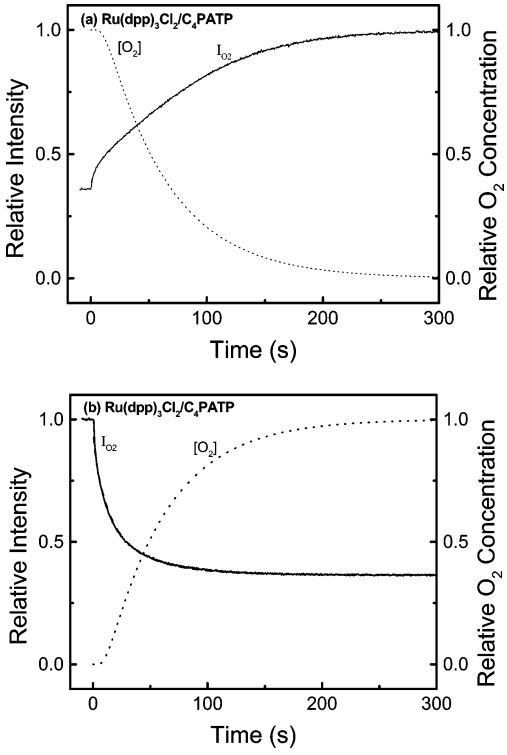

Figure 9. Intensity profiles of oxygen desorption (a) and sorption (b) obtained from the time-scan experiments on $Ru(dpp)_3Cl_2$ (100 ppm) in a C_4PATP film (0.162 mm thick). The solid curves refer to experimental data, whereas the overlapping dasheds line were simulated using assumed values of D_{O_2} (sorption, $D_{O_2} = 3.57 \times 10^{-6}$ cm^2 s^{-1}; desorption, $D_{O_2} = 4.78 \times 10^{-6}$ cm^2 s^{-1}). The plots of oxygen concentration were obtained with these values of D_{O_2} by integrating eq 3b over the film thickness.

(relative error < 5%) than when different film samples are compared (error < 30%). This indicates the possible non-uniformity of film thickness and/or errors in the thickness measurement.

Similar behavior can also be observed in the time-scan plots of PtTFPP/C_4PATP films (Figure 8). From 12 measurements on 3 films, we obtained an average value of $D_{O_2} = (4.0 \pm 1.0) \times 10^{-6}$ cm^2 s^{-1}. Within experimental error, this value is close to the value of $D_{O_2} = (3.7 \pm 1.0) \times 10^{-6}$ cm^2 s^{-1} determined from PtOEP/C_4PATP films. The time-scan experimental results of a C_4PATP film containing $Ru(dpp)_3Cl_2$ are shown in Figure 9a,b. In the oxygen-desorption experiment (Figure 9a), the increase of emission intensity occurs over 350 s, but for the oxygen-sorption experiment, the intensity decreases over 200 s. On the basis of five separate experiments, with films ranging in thickness from 0.135 mm to 0.220 mm, we obtain an average value of $D_{O_2} = (3.7 \pm 0.7) \times 10^{-6}$ cm^2 s^{-1}. Thus there is little variation in D_{O_2} values obtained from time-scan experiments carried out with different dyes.

Discussion

Oxygen quenching is a dynamic process. In Figure 4 we saw that plots of $\tau^\circ/\langle\tau\rangle$ and I°/I were coincident for all three dyes. If static quenching were significant, one would see differences in the lifetime and intensity Stern−Volmer plots. In Figures 7−9 we see that there is good agreement between the intensity profiles measured in experiments and those simulated according to eqs 1−4. These results confirm that oxygen diffusion in C_4-PATP obeys Fick's laws. The values of D_{O_2} in C_4PATP obtained from time-scan experiments on films containing the three

TABLE 1: Comparisons of the Values of D_{O_2}, P_{O_2}, S_{O_2}, and αR_{eff} for Different Dyes in C_4PATP, Calculated from Time-Scan and Time-Resolved Experiments at 22 °C

permeation parameters[a]		PtOEP	PtOEPK	PtTFPP	$Ru(dpp)_3Cl_2$
time-scan (intensity)	D_{O_2}	3.7		4.0	3.7
	P_{O_2}	3.9		2.6	1.8
	S_{O_2}	1.0		0.63	0.49
time-resolved (lifetime)	D_{O_2}	3.7	3.7[c]	4.0	3.7
	P_{O_2}	4.0 (3.7)[b]	3.62	2.6	2.0
	S_{O_2}	1.1 (1.0)	0.98	0.63	0.54
	αR_{eff}	1.0[d]	1.0	0.65	0.5

[a] Units: D_{O_2} 10^{-6} cm^2 s^{-1}; S_{O_2}, 10^{-3} M atm^{-1}; P_{O_2}, 10^{-12} mol s^{-1} cm^{-1} atm^{-1}; αR_{eff}, nm. [b] Values in parentheses are for experiments repeated one year later, at the same time as for the experiments with PtOEPK. [c] Value of D_{O_2} assumed for the calculation of S_{O_2}. [d] Assumed value. The values for the other dyes were calculated from the ratio $(P_{O_2})_{dye}/(P_{O_2})_{PtOEP}$.

different luminescent dyes as probes yield identical values of D_{O_2} within experimental error (Table 1). This is a satisfying result, since D_{O_2} is a property only of the polymer matrix.

We also expect similar values of the oxygen permeability from these experiments. Values of $P_{O_2} = D_{O_2}S_{O_2}$ can be obtained in two ways. Because plots of $\langle\tau\rangle^\circ/\langle\tau\rangle$ and I°/I vs p_{O_2} are linear (and superimpose), P_{O_2} values can be calculated from the slopes. In addition, one can calculate values of the permeability according to eq 2 from the B parameters obtained in time-scan experiments. Table 1 lists the values of P_{O_2} obtained from both types of experiments. For each dye, values of P_{O_2} obtained from the two different measurements are the same within experimental error. For PtOEPK, we carried out only time-resolved phosphorescence decay measurements. Here the calculated P_{O_2} value is very close to that obtained with PtOEP. In contrast, the permeability values for PtTFPP and $Ru(dpp)_3Cl_2$ are significantly different from those of PtOEP or PtOEPK. Differences in the values of $P_{O_2} = D_{O_2}S_{O_2}$ are our first indication of differences in the interaction of oxygen with the excited states of the different dyes.

These calculations depend on prior knowledge of the product of the probability parameter and the capture radius αR_{eff} in eqs 1 and 2. The P_{O_2} values were calculated assuming that $\alpha = 1$ and $R_{eff} = 1.0$ nm. Although α is expected to be unity for quenching of singlet excited states,[11] several authors[12] have argued that α is at most 1/9 for phosphorescence quenching by oxygen. The way in which spin statistics enter into triplet quenching is rather subtle, and many authors simply set α equal to unity in analyzing their data. For example, in the theory of partially diffusion-controlled reactions,[13] α increases as the diffusion coefficient of quenchers decreases. Our finding that P_{O_2} values depend on the choice of dye indicates that our assumption that $\alpha R_{eff} = 1.0$ nm is incorrect.

The apparent difference in P_{O_2} and S_{O_2} values can be reconciled if we assume that αR_{eff} for O_2 quenching depends on the dye. We can obtain identical values of these polymer parameters if we adjust the value of αR_{eff} to 0.65 nm for PtTFPP/C_4PATP and 0.5 nm for $Ru(dpp)_3Cl_2$/C_4PATP. These differences might arise as a consequence of differences in molecular structure and steric effects associated with the ligands of each dye.

Sorption vs Desorption Time-Scan Experiments. We end with a brief discussion of the factors that affect the difference in the time response in oxygen-sorption and -desorption experiments. The data in Figure 4 indicate that dyes with longer lifetimes (50−100 μs), such as PtOEP or PtTFPP, have much greater sensitivity to low oxygen partial pressures than dyes with shorter lifetimes such as $Ru(dpp)_3Cl_2$. When long-lifetime dyes are used in time-scan measurements to determine oxygen diffusion rates (Figures 7 and 8), we find that oxygen-desorption measurements provide more precise values of D_{O_2} than oxygen-sorption measurements. For films exposed to an increase in oxygen pressure, the drop in luminescence intensity is very rapid, and there are fewer meaningful data points to analyze. In contrast, for dyes with short lifetimes, there are much smaller differences in the time scales for the sorption and desorption experiments (Figure 9). To provide a deeper understanding of the origin of this effect, we take the values of D_{O_2} characterizing each curve and then integrate eq 4a over the film thickness L to calculate the mean oxygen concentration ($[O_2]_{av}$) in the film as a function of time.

In Figure 7a,b we plot the relative oxygen concentration ($[O_2]_{rel} = [O_2]_{av}/[O_2]_{eq}$) corresponding to the time-scan experiment. In the oxygen-desorption experiment, there is a rapid decrease in $[O_2]_{rel}$ over the first 50 s, but the remaining oxygen is still effective at quenching emission. The growth in luminescence intensity is more sensitive to the later stages (50−120 s) of oxygen diffusion out of the film. In the oxygen-sorption experiment, the growth in $[O_2]_{rel}$ occurs over 50 s, but the small fraction of the final $[O_2]_{t=150s}$ that enters the film during the first 10 s is effective at quenching emission. Similar results are obtained for PtTFPP/C_4PATP, as seen in Figure 8.

In contrast, the decrease in luminescence intensity for oxygen sorption into a $Ru(dpp)_3Cl_2$/C_4PATP film is less precipitous. As can be seen in Figure 9b, the decrease takes place over about 50 s. The fractional quenching reaches about 90% when $[O_2]_{rel}$ reaches about half of its final value. This difference in behavior is a consequence of the shorter luminescence lifetime (6.2 μs) of the Ru dye. Oxygen in the film is less efficient at quenching its luminescence. Relative to the intensity at zero oxygen pressure, the quenched intensity of $Ru(dpp)_3Cl_2$ in the film in the presence of air is higher than that of PtOEP by a factor of ca. 15.

Heterogeneous Quenching Kinetics of Dyes in C_4PATP. In this section, we look more deeply at the origin of the nonexponential luminescence decays for PtOEP and PtTFPP in C_4PATP in the presence of oxygen and compare the behavior with that of $Ru(dpp)_3Cl_2$. As we mentioned in the Introduction, the nonexponential decay profiles for the neutral Pt−porphyrin dyes are unexpected. One expects that the polymer chains in the bulk state at temperatures well above T_g will undergo local relaxation on a time scale much faster than the dye excited state, particularly for phosphorescence.

To proceed with our analysis, we first fitted the decay profiles of PtOEP in C_4PATP (Figure 3) to a sum of two exponential terms to examine whether the individual parameters have meaning. In the expression

$$\frac{I(t)}{I(0)} = A_{sh}\exp\left(-\frac{t}{\tau_{sh}}\right) + A_l\exp\left(-\frac{t}{\tau_l}\right) \qquad (7)$$

A_{sh} and τ_{sh} refer to the short τ component and A_l and τ_l refer to the long τ component. We plot the pressure dependence of these parameters in Figure 10 and make the remarkable observation that the preexponential terms A_{sh} and A_l are constant over the entire range of $p_{O_2} > 0$ examined, whereas the individual fitted lifetimes exhibit a simple Stern−Volmer behavior. The A_{sh} value (ca. 95%) is much larger than the A_l value (ca. 5%). This type of result is consistent with a model in which there are two kinds of sites for the dye in the matrix, and the dye does not migrate between these types of sites during its excited-state lifetime. Another interesting feature of this plot is that the slope of the

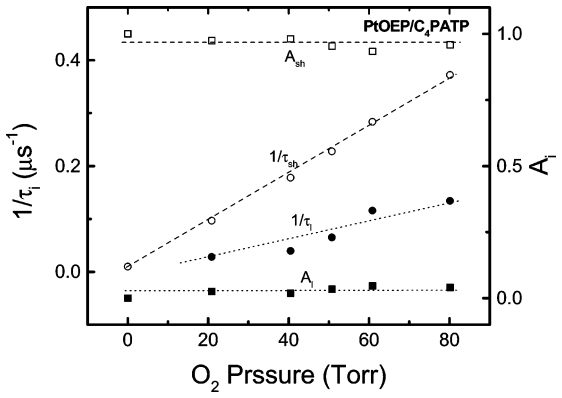

Figure 10. Oxygen partial pressure dependence of the parameters A_{sh}, A_l, τ_{sh}, and τ_l obtained from fitting the decay profiles of PtOEP in C_4-PATP to eq 7: $I(t)/I(0) = A_{sh}\exp(-t/\tau_{sh}) + A_l\exp(-t/\tau_l)$.

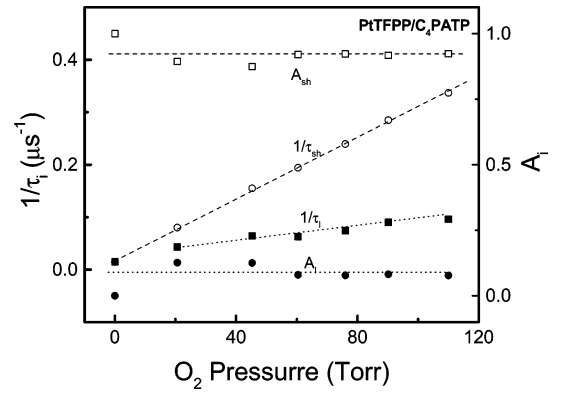

Figure 11. Oxygen partial pressure dependence of the parameters A_{sh}, A_l, τ_{sh}, and τ_l obtained from fitting the decay profiles of PtTFPP in C_4PATP to eq 7.

$1/\tau_{sh}$ plot is steeper than that of the $1/\tau_l$ plot, indicating that the dyes in the short lifetime sites are more sensitive to the O_2 pressure change.

Equation 1 can be rewritten as

$$\frac{1}{\tau} = \frac{1}{\tau^\circ} + k_q S_{O_2} p_{O_2} \tag{8}$$

The oxygen-quenching rate constant (k_q) can be calculated from the slope of the plot of $1/\tau$ vs p_{O_2}. We begin by assuming that the oxygen molecules are uniformly distributed in the C_4PATP matrix, so that the oxygen solubilities in the polymer associated with the two types of sites are identical. Using the value of $S_{O_2} = 1.0 \times 10^{-3}$ M atm^{-1} (Table 1), calculated from the experiments on PtOEP/C_4PATP, we obtained a k_q value of 3.4×10^9 M^{-1} s^{-1} for the τ_{sh} sites and 1.2×10^9 M^{-1} s^{-1} for the τ_l sites. This result shows that molecular oxygen quenches the dye in the τ_{sh} sites at a faster rate than for the dye in the τ_l sites. While the exact meaning of this result is not clear, it might imply that the magnitude of αR_{eff} is larger for the τ_{sh} sites.

When this model was used to analyze the decay profiles of PtTFPP in C_4PATP, a similar result was obtained (Figure 11). Both A_{sh} and A_l are insensitive to the oxygen pressure change. The individual values of k_q for this dye are smaller than those for PtOEP for both the τ_{sh} and τ_l sites.

$Ru(dpp)_3Cl_2$ in C_4PATP behaves differently. Recall that the phosphorescence decay of this dye is nonexponential even in the absence of oxygen, behavior that we believe is typical for ionic dyes in polymer matrixes. Individual decay curves at all oxygen pressures can be fitted to a sum of two exponential terms. While the preexponential parameters (A_{sh} and A_l) were

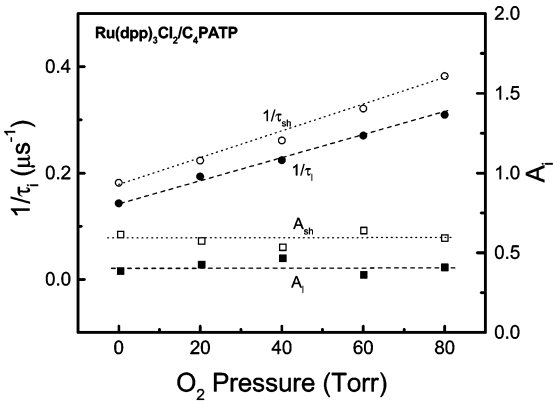

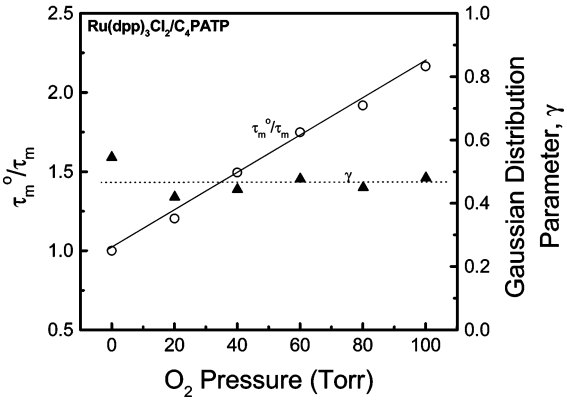

Figure 12. Oxygen partial pressure dependence of the parameters obtained from fitting the decay profiles of $Ru(dpp)_3Cl_2$ in C_4PATP to different models. (a) Values of A_{sh}, A_l, τ_{sh}, and τ_l obtained from the fits to a sum of two exponential terms. (b) Values of the mean lifetime τ_m and the distribution parameter γ, obtained from fitting the decays (Figure 6) to the Gaussian distribution of lifetimes model.

constant over the oxygen pressure range of 0−80 Torr (Figure 12a), the individual lifetimes were not consistent with the simple two-site model. Both $1/\tau_{sh}$ and $1/\tau_l$ increased linearly with increasing oxygen pressure, but neither line extrapolated through the origin. Both lines had similar slopes. Under these circumstances, a more appropriate model to describe this system is one that considers a distribution of lifetimes for the excited dye.

We tested this idea by fitting the individual decays at different oxygen pressures in Figure 6 to a model assuming there is a Gaussian distribution of deactivation rates.[14] The distribution is characterized by a mean rate constant k_m ($=1/\tau_m = 1/\tau_m^\circ + k_{qm}[O_2]$) and a distribution parameter, γ. The term k_m is the average quenching constant over the distribution of excited-state dye microenvironments, which influence both τ_m° and k_q. The dispersion in the first-order rate constants for $-\infty \le x \le \infty$ then becomes

$$\ln(k) = \ln(k_m) + \gamma x \tag{9}$$

The observed decay profile is composed of the summation of the contributions from each microscopic species. Integration over the distribution $\exp(-x^2)$ yields the following equation when the luminescence intensity is proportional to the dye's excited-state concentration

$$\frac{I(t)}{I(0)} = \frac{\int_{-\infty}^{\infty}\exp(-x^2)\exp[-k_m x\exp(\gamma x)]\,dx}{\int_{-\infty}^{\infty}\exp(-x^2)\,dx} \tag{10}$$

where $\int_{-\infty}^{\infty}\exp(-x^2)\,dx = \pi^{1/2}$ and x is the integration variable.

These equations were evaluated using the methods described in ref 14. Individual decay traces fit equally well to the Gaussian distribution model and to a sum of two exponentials, as characterized by the goodness of fit and a random distribution of weighted residuals. Plots of τ_m°/τ_m and γ against p_{O_2} are presented in Figure 12b. The lifetime ratio plot is linear, with an intercept of 1, and $\tau_m^\circ = 5.65\ \mu s$. The distribution parameter γ is essentially independent of the oxygen concentration in the C_4PATP matrix. Its value is about 0.45. This result indicates that there is a distribution of the rate constants for deactivation of $Ru(dpp)_3Cl_2$ in a C_4PATP medium, and the breadth of this distribution is not greatly affected by the presence of oxygen.

For completeness, we used the Gaussian distribution model to analyze the decays of PtOEP and PtTFPP in C_4PATP. The fitting was poor. Individual fits to decay curves for both PtOEP and PtTFPP were characterized by a nonrandom distribution of weighted residuals. We conclude that these dyes in C_4PATP are better characterized by two sites with discrete lifetimes.

Summary

The time-scan experimental results for PtOEP/C_4PATP, PtTFPP/C_4PATP, and $Ru(dpp)_3Cl_2$/C_4PATP show that oxygen diffusion in C_4PATP obeys Fick's laws with a diffusion coefficient of $(3.7 \pm 1.0) \times 10^{-6}\ cm^2\ s^{-1}$. For PtOEP, the values of oxygen permeability calculated from intensity and lifetime Stern−Volmer plots are identical, equal to 4.0×10^{-12} mol $cm^{-1}\ s^{-1}\ atm^{-1}$, and very similar to that calculated from a lifetime Stern−Volmer plot for PtOEPK in C_4PATP. These values are larger than those obtained from similar measurements on PtTFPP and $Ru(dpp)_3Cl_2$ in C_4PATP. To reconcile apparent differences in P_{O_2} values, we conclude that (αR_{eff}) for oxygen quenching of $Ru(dpp)_3Cl_2$ is half the value, and that for PtTFPP is 0.65 of the value for oxygen quenching of PtOEP and PtOEPK.

PtOEP, PtOEPK, and PtTFPP in C_4PATP exhibit exponential decays in the absence of oxygen. In contrast, the decays of $Ru(dpp)_3Cl_2$ in C_4PATP are always nonexponential. The heterogeneity of the decay times for $Ru(dpp)_3Cl_2$ in C_4PATP can be described by a continuous distribution model of dye lifetimes (i.e., a Gaussian distribution). The width of this distribution shows no dependence of oxygen pressure. The nonexponential decays for platinum dyes (PtOEP and PtTFPP) in C_4PATP at elevated p_{O_2} do not fit to the Gaussian distribution model. Rather there appear to be two discrete classes of sites with independent lifetimes and different sensitivities to oxygen quenching for dyes in these sites. For this explanation to be valid, it is necessary that the dyes do not exchange between the two different types of sites on the time scale of their excited-state lifetimes (ca. 100 μs).

Acknowledgment. We thank NSERC Canada and Materials and Manufacturing Ontario (MMO) for their support of this research.

References and Notes

(1) (a) Hartman, P.; Trettnak, W. *Anal. Chem.* **1996**, *68*, 2615−2620. (b) Papkovsky, D. B.; Ovchinnikov, A. N.; Ogurtsov, V. I.; Ponomarev, G. V.; Korpela, T. *Sens. Actuators B* **1998**, *51*, 137−145. (c) Papkovsky, D. B. *Sens. Actuators B* **1995**, *29*, 213−218. (d) Mills, A. *Sens. Actuators B* **1998**, *51*, 60−68. (e) Mills, A. *Sens. Actuators B* **1998**, *51*, 69−76. (f) Eaton, K.; Douglas, P. *Sens. Actuators* **2002**, *82*, 94−104. (g) Douglas, P.; Eaton, K. *Sens. Actuators* **2002**, *82*, 200−208.

(2) (a) Gouterman, M. *J. Chem. Educ.* **1997**, *74*, 697. (b) Bell, J. H.; Schairer, E. T.; Hand, L. A.; Mehta, R. D. *Annu. Rev. Fluid Mech.* **2001**, *33*, 155.

(3) Lu, X.; Winnik, M. A. In *Luminescence Quenching in Polymer Films*; Ramamurthy, V., Schanze K. S., Eds.; Molecular and Supramolecular Photochemistry; Marcel-Dekker: New York, 2000; Vol. 6, pp 311−352.

(4) Lakowicz, J. R. *Principles of Fluorescence Spectroscopy*; Kluwer Academic/Plenum Publishers: New York, 1999.

(5) (a) Liang, M.; Manners, I. *J. Am. Chem. Soc.* **1991**, *113*, 4044. (b) Ni, Y.; Stammer, A.; Liang, M.; Massey, J.; Vancso, G. J.; Manners, I. *Macromolecules* **1992**, *25*, 7119. (c) Ni, Y.; Park, P.; Liang, M.; Massey, J.; Waddling, C.; Manners, I. *Macromolecules* **1996**, *29*, 3401.

(6) (a) Raja, A. V.; Lagowski, J. B. *Comput. Theor. Polym. Sci.* **1996**, *6*, 79. (b) Jaeger, R.; Lagowski, J. B.; Manners, I.; Vancso, G. J. *Macromolecules* **1995**, *28*, 539.

(7) Jayarajah, C. N.; Yekta, A.; Manners, I.; Winnik, M. A. *Macromolecules* **2000**, *33*, 5693.

(8) Pang, Z.; Gu, X.; Yekta, A.; Masoumi, Z.; Coll, J. B.; Winnik, M. A.; Manners, I. *Adv. Mater.* **1996**, *8*, 768.

(9) Lin, C. T.; Böttcher, W.; Chow, M.; Crentz, C.; Sutin, N. *J. Am. Chem. Soc.* **1976**, *98*, 6536.

(10) (a) Yekta, A.; Masoumi, Z.; Winnik, M. A. *Can. J. Chem.* **1995**, *73*, 2021. (b) Masoumi, Z.; Stoeva, V.; Yekta, A.; Pang, Z. Manners, I.; Winnik, M. A. *Chem. Phys. Lett.* **1996**, *261*, 551.

(11) Nowakowska, P. F.; Najbar, J.; Waligora, B. *Eur. Polym. J.* **1976**, *12*, 387.

(12) (a) Gijzeman, O. L. J.; Kaufman, F.; Porter, G. J. *Chem. Phys. Lett.* **1970**, *69*, 708. (b) Patterson, L. K.; Porter, G.; Topp, M. R. *Chem. Phys. Lett.* **1970**, *7*, 612. (c) Guillet, J. E.; Andrews, M. *Macromolecules* **1992**, *25*, 2752.

(13) Collins, F. C.; Kimball, G. E. *J. Colloid. Sci.* **1949**, *4*, 425.

(14) Krasnansky, R.; Koike, K.; Thomas, J. K. *J. Phys. Chem.* **1990**, *94*, 4521.